Open Access

CrossMark

Influence of Atomic Hydrogen, Band Bending, and Defects in the Top Few Nanometers of Hydrothermally Prepared Zinc Oxide Nanorods

Mubarak J. Al-Saadi[1], Salim H. Al-Harthi[1*], Htet H. Kyaw[1], Myo T.Z. Myint[1], Tanujjal Bora[2], Karthik Laxman[2], Ashraf Al-Hinai[3] and Joydeep Dutta[4]

Abstract

We report on the surface, sub-surface (top few nanometers) and bulk properties of hydrothermally grown zinc oxide (ZnO) nanorods (NRs) prior to and after hydrogen treatment. Upon treating with atomic hydrogen (H*), upward and downward band bending is observed depending on the availability of molecular H_2O within the structure of the NRs. In the absence of H_2O, the H* treatment demonstrated a cleaning effect of the nanorods, leading to a 0.51 eV upward band bending. In addition, enhancement in the intensity of room temperature photoluminescence (PL) signals due to the creation of new surface defects could be observed. The defects enhanced the visible light activity of the ZnO NRs which were subsequently used to photocatalytically degrade aqueous phenol under simulated sunlight. On the contrary, in the presence of H_2O, H* treatment created an electronic accumulation layer inducing downward band bending of 0.45 eV (~1/7th of the bulk ZnO band gap) along with the weakening of the defect signals as observed from room temperature photoluminescence spectra. The results suggest a plausible way of tailoring the band bending and defects of the ZnO NRs through control of H_2O/H* species.

Keywords: ZnO, Band bending, Surface defects, Hydrogen treatment, Visible light photocatalysis

Background

Zinc oxide (ZnO) is a wide band gap semiconductor material with a band gap of about 3.4 eV and a large exciton binding energy at room temperature (60 meV) [1, 2]. It has unique optical and electrical properties and can be grown in various morphologies using low-cost synthesis techniques [3]. It has been reported that well-ordered ZnO grains with fewer defects show better optical properties compared to the large discrete islands or structure less overgrowth based on flat continuous layers [4]. Microshape dependency shows that ZnO nanorods (NRs) have the best optical properties among nanoshells and nanoneedles [5]. In contrast, it has been also reported that enhanced surface defects play a crucial role in ZnO nanostructures when it is used as a visible light photocatalyst [6–9].

The method to enhance the optical properties of ZnO NRs has involved annealing in air [10], hydrogen treatment [11], and annealing in various environments [12, 13]. Yanob et al. showed that hydrogen is responsible for the near-band edge enhancement and drastic increment in the conductivity of the ZnO nanowires [11]. Ching-Ming Hsu et al. reported that the conductivity of thin films of molybdenum-doped zinc oxide was increased by a factor of 4 when treated by hydrogen over a period of 30 min [14]. Furthermore, hydrogen treatment of ZnO NRs can be used to control the electronic and optical properties of ZnO by creating defects within the ZnO crystal [15, 16]. These defects can be in the form of oxygen vacancies which act as deep donors, zinc vacancies as deep acceptors, zinc interstitials as shallow donors, oxygen interstitials as

* Correspondence: salim1@squ.edu.om
[1]Department of Physics, Sultan Qaboos University, PO Box 36, Al Khoudh, 123, Muscat, Oman
Full list of author information is available at the end of the article

Al-Saadi *et al. Nanoscale Research Letters* (2017) 12:22

Page 2 of 11

deep accepters at the octahedral site, oxygen anti-sites as deep accepters, and zinc anti-sites as shallow donors [17]. However, existence of a certain type of defect depends on the surrounding environment during the preparation or post-treatment of the ZnO NRs. Additionally, the formation and density of these defects is partly dependent on the chemical composition of the samples, wherein recent studies have shown that the presence of H_2O can play a part in directing the defect formation [18]. A recent study by Gutmannet et al. [19] demonstrated the effect of annealing, ambient exposure, and photon flux-induced artifacts on work function Φ measurements of the nanocrystalline ZnO surfaces. The authors used ultraviolet photoemission spectroscopy (UPS) and low intensity X-ray photoemission spectroscopy (LIXPS) to determine the absolute Φ values and to confirm the hypothesis that surface hydroxylation by photo-induced H_2O dissociation is most likely responsible for 0.30–0.35 eV Φ reduction of the band gap observed during UPS measurements. Their results suggest that any UPS measurements on ZnO surfaces exposed to ambient or H_2O should consider 0.30–0.35 eV correction factor to determine the Φ accurately. Another study by Kumar Kumarappan [20] reported on the effect of H* cleaning on single ZnO (0001) crystal and associated upward band bending after partial removal of the surface contaminants at elevated temperature. Heinhold et al. [21] showed the influence of polarity and hydroxyl termination on the band bending at ZnO surfaces. Their results indicated how the Fermi level (E_f) could be reversibly cycled between the conduction band and the band gap (E_g) by controlling the surface H coverage using simple ultra-high vacuum (UHV) heat treatments up to 750 °C, dosing with H_2O/H_2 and atmospheric exposure. In addition, they demonstrated the upward and downward surface band bending (V_{sbb}) upon annealing of the H_2O/H_2 dosed O and Zn-polar faces of ZnO single-crystals.

Despite of the aforementioned efforts, hydrogenation of ZnO leads to effects which are not yet fully understood and explored. For example, in addition to the ambiguous electronic effects attributed to the hydrogen treatment of ZnO, it is unclear how the intrinsic H_2O content due to the ZnO NRs soft chemistry preparation interacts with H* in the top few nanometers at room temperature—this is different from the abovementioned studies which were based on annealing of the H_2O/H_2 dosed O and Zn-polar faces of ZnO single-crystals. In addition to that and to the best of our knowledge, there are no reports on the effects of the electronic structure variation—such as band bending—in pristine- and hydrogen-treated ZnO NRs.

In this work, we report on the preparation of ZnO NRs on glass substrate by a simple hydrothermal process. The effect of trapped H_2O molecules on the band bending at the surface of the ZnO NRs is probed using XPS and UPS. The effect of H* treatment on the samples with and without intrinsic H_2O molecules is also explored in terms of band bending and defect-induced photoluminescence (PL) intensities. The correlation between oxygen vacancies with PL intensities and valence band maximum (E_{VBM}) of ZnO NRs with and without trapped H_2O molecules are further discussed.

Experimental
Materials
The ZnO NRs were synthesized using the following materials: Analytical grade zinc acetate dihydrate (Zn $(CH_3COO)_2\cdot2H_2O$) was purchased from MERCK, Germany, and zinc nitrate hexahydrate (Zn $(NO_3)_2\cdot6H_2O$) and hexamethylenetetramine ($(CH_2)_6N_4$) were obtained from Sigma-Aldrich, USA. All the chemicals were used without further purification. Standard microscope glass slides were used as substrates for the growth of ZnO NRs, which were cleaned in ultrasonic water bath using soap water, acetone, ethanol, and deionized (DI) water prior to the growth of the nanorods.

Methods
Substrate Seeding with ZnO Nanocrystallites
ZnO nanocrystallites were seeded on glass substrates using 10 mM solution of zinc acetate dihydrate in 20 mL dissolved in DI water followed by spraying on pre-heated (350 °C) substrates [22, 23]. After spraying, the samples were annealed at 350 °C for 5 h in the ambient and stored in an oven at 90 °C until further use. The purpose of ZnO seeding was to augment nucleation sites for ZnO NRs growth [24, 25].

Hydrothermal Synthesis of ZnO NRs
ZnO NRs were grown on the pre-seeded glass substrates by following facile hydrothermal process as reported in previous works [26, 27].

Briefly, the seeded glass substrates were placed in a solution with equimolar concentrations (20 mM) of zinc nitrate hexahydrate and hexamethylenetetramine (precursor solution) and then kept in an oven at 90 °C. The growth process was carried out for 10 h, and precursor solution was replenished after 5 h to maintain a constant growth rate for the nanorods [26]. Then, the samples were thoroughly rinsed with DI water and annealed at 350 °C in ambient air to remove any un-reacted chemicals on the surface. The positioning of the glass slide inside the furnace and annealing temperature were crucial to engineer portions of ZnO NRs with and without H_2O on the same glass slide simultaneously. These portions

Al-Saadi *et al. Nanoscale Research Letters* (2017) 12:22

Page 3 of 11

were identified by XPS before commencing of any experiment.

Atomic Hydrogen Treatment

Hydrogen treatment was carried out using hydrogen cracking cell from Omicron (Fig. 1c). The efficiency of cracking was almost 10%. The hydrogen gas pressure was kept stable at 10^{-6} mbar for 2 h which resulted in the sample hydrogen exposure of about 7.2 KL (1KL = 7.2×10^{-3} mbar.s).
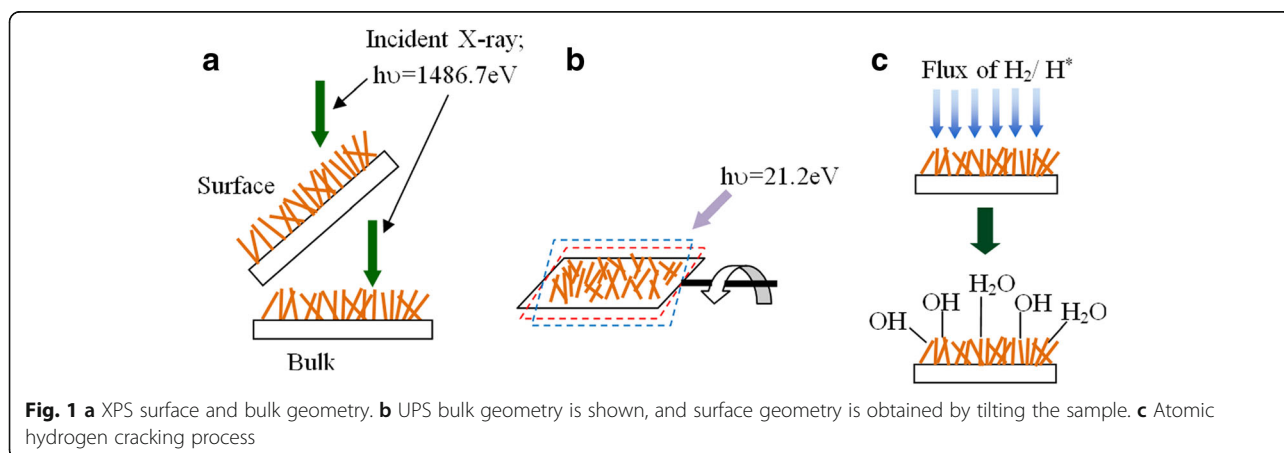
Characterization

Surface morphology of ZnO NRs on glass substrates was characterized by JEOL JSM-7800F (Japan) field emission scanning electron microscope (FESEM) working at 30 kV. X-ray photoemission spectroscopy (XPS) (Omicron Nanotechnology, Germany) with a monochromatic Al Kα radiation (hν = 1486.6 eV) working at 15 kV was used for surface, sub-surface, and bulk analysis of ZnO NR samples before and after the hydrogen treatment. Figure 1a shows experimental geometry used for XPS investigations. The obtained XPS spectra were deconvoluted to individual components using Gaussian Lorentzian function with Casa XPS software and calibrated with respect to the C 1s feature at 284.6 eV. During the XPS experiments, all the measured samples were flooded with electrons to neutralize surface charging effects. Ultraviolet photoelectron spectroscopy (UPS) (Omicron Nanotechnology, Germany) with radiation energy of (21.2 eV) was used for surface and sub-surface density of state analysis of ZnO nanorods samples before and after hydrogen treatment by changing the sample tilt angle as depicted in Fig. 1b. In order to measure changes in the ZnO Φ due to hydrogen treatment, UPS was calibrated and tested using ITO thin film following the procedure adopted by Park et al. [28]. X-ray diffraction (XRD) of ZnO NRs were obtained by using a Rigaku MiniFlex600 X-ray diffractometer with

Cu Kα X-ray radiation (wavelength = 1.54 Å). Room temperature photoluminescence (PL) of the NRs were recorded in a Perkin Elmer LS55 fluorescence spectrometer with an excitation wavelength of 325 nm. Photocatalytic activity test was carried out on H* untreated and H* ZnO samples soaked in 10 ppm phenol solution. The phenol degradation was done under simulated solar light (AM 1.5 radiation, 1 kW/m^2), and the phenol degradation kinetics were studied by using ultra performance liquid chromatography (UPLC, LC-30AD, Shimadzu, Tokyo, Japan) technique.

Results and Discussion

Scanning electron micrographs of as-prepared ZnO NRs grown on glass substrates were observed to have an average diameter and length of 120 ± 10 nm and 3.5 ± 0.2 μm, respectively (Fig. 2a). X-ray diffraction (XRD) analysis of the as-grown samples showed the hexagonal wurtzite structure of the ZnO crystal as confirmed by the 2θ values at 31.8, 34.4, 36.2, 47.4, 62.9, and 72.7 (JCPDS card no. 01-089-0510) corresponding to (100), (002), (101), (102), (103), and (104) crystal planes, respectively, as observed in Fig. 2b [26, 29]. The strongest XRD peak at 34.35° indicates the preferred growth of the rods along (002) crystal direction. Some of the as-prepared ZnO NRs were observed to have chemisorbed H_2O and some did not as is indicated by an increase of 0.2 eV in XPS binding energy for the Zn 2p peak—for the sample with H_2O—which results from the spin orbital splitting of the Zn 2p core ionization peak as shown in Fig. 2c [30].

To better understand the surface composition of the NRs, the oxygen (O 1s) peaks of the as prepared samples with and without chemisorbed H_2O molecules were studied using XPS. As shown in Fig. 2d, asymmetric O 1s peak of the sample without H_2O on the surface could be coherently fitted by two Gaussian components, centered at 529.7 eV (O_a) and at 531.0 eV (O_b). An

Fig. 1 **a** XPS surface and bulk geometry. **b** UPS bulk geometry is shown, and surface geometry is obtained by tilting the sample. **c** Atomic hydrogen cracking process
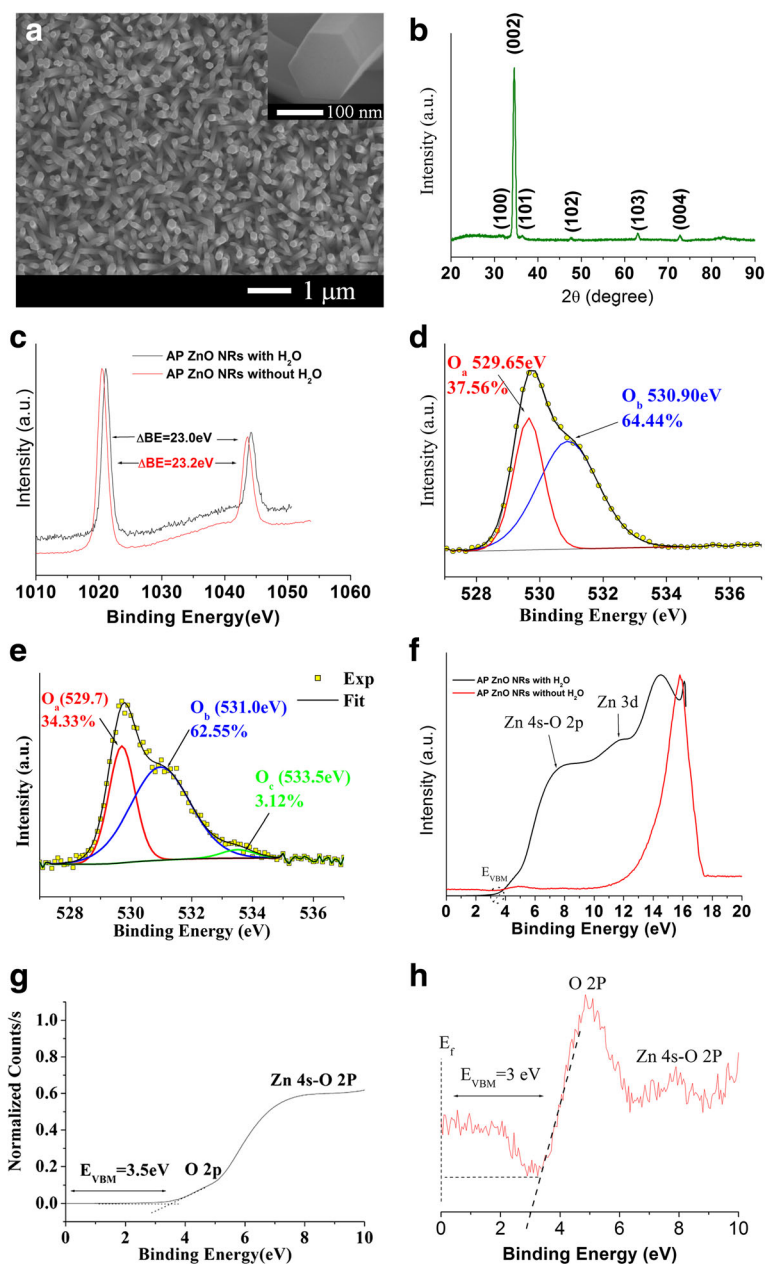
Fig. 2 **a** Scanning electron micrograph of ZnO NRs (*inset*: magnified image of the hexagonal structure of a single crystal ZnO nanorod). **b** XRD spectrum of ZnO NRs. **c** Zn 2p XPS spectrum of the as prepared (AP) ZnO NRs with and without H_2O. **d** O 1s XPS spectrum of ZnO without H_2O. **e** O 1s XPS spectrum of ZnO with H_2O. **f** UPS spectra of ZnO NRs with and without H_2O samples. **g** UPS valence band region of ZnO with H_2O. **h** UPS valence band region of ZnO without H_2O

additional component at 533.5 eV (O_c) is found for the sample with H_2O as shown in Fig. 2e, attributed to chemisorbed H_2O species on NR surface. The O_a peak is attributed to lattice oxygen in wurtzite ZnO forming Zn–O bonding, while O_b is attributed to O^{2-} ions in oxygen-deficient regions within the ZnO matrix (oxygen vacancies) and the surface adsorbed loosely bonded oxygen like hydroxyls (OH) bonds, i.e., ZnO(OH) [31]. O_c can be ascribed to the specific chemisorbed oxygen,

from adsorbed CO_2, O_2, or H_2O [32]. The peak positions correspond well with literature, which show that the O_b and O_c peaks lie at approximately 1.35 and 3.8 eV to the right of the lattice oxygen peak in ZnO crystal [33]. In order to observe the effect of the chemisorbed H_2O species on the electronic properties of ZnO NRs, ultraviolet photoelectron spectroscopy (UPS) technique was employed as shown in Fig. 2f. An enhancement in the intensity of band structure features (i.e., the valence

Al-Saadi *et al. Nanoscale Research Letters* (2017) 12:22

Page 5 of 11

band maximum (E_{VBM}), Zn 4s-O 2p (~6–8 eV), and Zn 3d (~10.5–11.5 eV)) is observed for the ZnO sample which contains the chemisorbed species. Consequently, the E_{VBM} was found to be high (3.5 ± 0.1 eV) as estimated from the linear extrapolations of the foremost edges of the UPS data graphs depicted from Fig. 2g. It is noteworthy that the O 2p (~4.5 eV) ZnO-related surface state is absent in the UPS of the sample with H_2O but visible for the samples without H_2O with reduced E_{VBM} value of (3.0 ± 0.1 eV) as shown in Fig. 2h.

ZnO defects were investigated on samples with and without adsorbed H_2O species subjected to H^* treatment for 2 h. Figure 3a, b shows theZn 2p core level ionization peaks after the H^* exposure. It is clear from Fig. 3a that a significant reduction in the Zn peak is detected after hydrogen treatment for samples with H_2O on the surface. The results suggest that H^* either etches ZnO surface removing zinc ions from the crystal lattice or forms a layer on the surface of the rods which causes a reduction in the Zn intensity due to the reduction of the XPS sampling depth. The latter explanation is most likely responsible for the reduction of Zn peak intensity. This is supported by the Zn peak binding energy shift of 0.3 eV caused by the layer creating a surface potential (i.e., band bending) which is anticipated to change the Φ of the sample in the presence of surface H_2O. On the contrary, hydrogen treatment of the sample without H_2O shows both slight increase in the intensity (ΔI_o = 5%) of Zn and binding energy shift (0.14 eV) (Fig. 3b) suggesting cleaning process of ZnO surface by H^* to occur.

XPS depth profiling was carried out to get better insight of the distribution of defects in ZnO NRs treated by H^*. The schematic diagram showing experimental geometry indicates incident X-ray direction on ZnO sample as shown in Fig. 1a. The bulk characterization of O 1s peaks was achieved with X-rays perpendicular to the ZnO surface, while glancing angles provided surface and sub-surface information. Figure 4a–c shows the O

1s peak of ZnO nanorods without H_2O after treatment with H^* for 2 h. Upon moving from the surface to deep-bulk, we observe that O_b decreases while O_a increases and not surprisingly, no adsorbed H_2O species (i.e., O_c peak) was observed. Correspondingly, the O 1s signals obtained from the sample with H_2O (Fig. 4d–f) show existence of O_a, O_b, and O_c components on the surface and in bulk regions. O_c depletion layer is also found at sub-surface region of the sample as seen in Fig. 2e. This confirms the presence of H_2O (i.e., O_c ~ 4.15%) on the ZnO NRs surface and in the bulk ZnO crystal (O_c ~ 10.18%), sandwiching the depletion layer.

Auxiliary experiments (not shown here) of Ar ion beam sputtering of 5 keV or annealing at 500 °C for 1 h of the ZnO NRs lead to the removal effect of the bulk H_2O content. A careful comparison between O 1s peaks for the sample without H_2O after hydrogen treatment and before (i.e., comparison between Figs. 4a and 2d) reveals that H^* treatment has an effect in the reduction of O_b (from 64.4 to 59%) and increase of the binding energy of the O 1s (from 529.7 to 530.8 eV for O_a and from 530.9 to 531.0 eV for O_b), therefore supporting the cleaning effect to take place due to the H^* treatment.

Despite an increase in the binding energy of O 1s obtained for the sample which contains H_2O, O_b tends to increase as seen from the comparison between Figs. 2e and 4d. The increase in binding energy observed for O 1s (0.3–0.4 eV) and Zn $2p_{3/2}$ (0.2 eV) peaks after hydrogen treatment suggests weakening of the Zn–O bond in the crystal lattice, which can increase the nuclear attraction force experienced by the electron, resulting in the increase of binding energy for both lattice oxygen and zinc.

The effect of hydrogen treatment on the electronic properties of samples without H_2O and with H_2O was investigated by UPS and by XPS valence data. Figure 5 shows the UPS and XPS valence band spectrum obtained for the sample without H_2O. Before hydrogen treatment, all ZnO surface states (O 2p (~4.5 eV), Zn
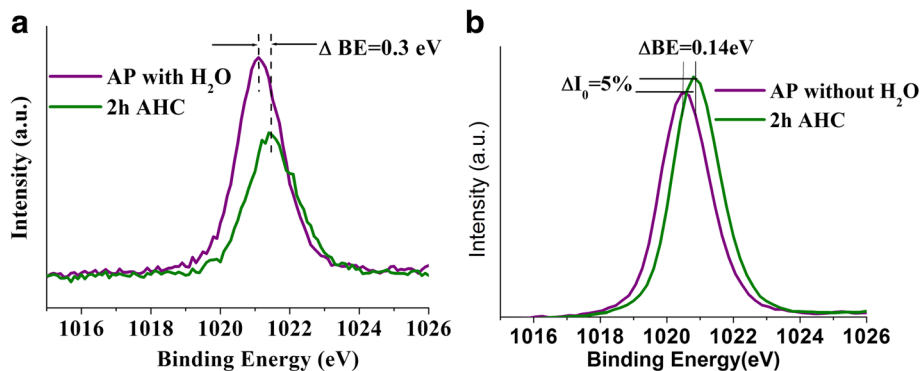

Fig. 3 Normalized Zn 2p XPS spectrum of as-prepared ZnO NRs with (**a**) and without (**b**) H_2O before and after hydrogen treatment for 2 h

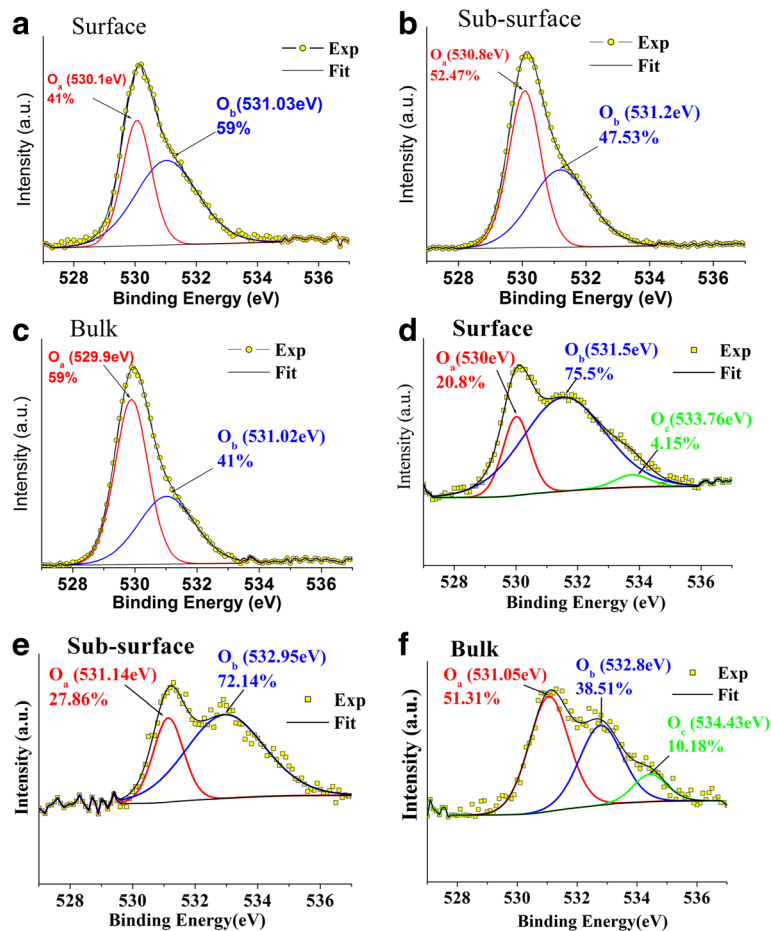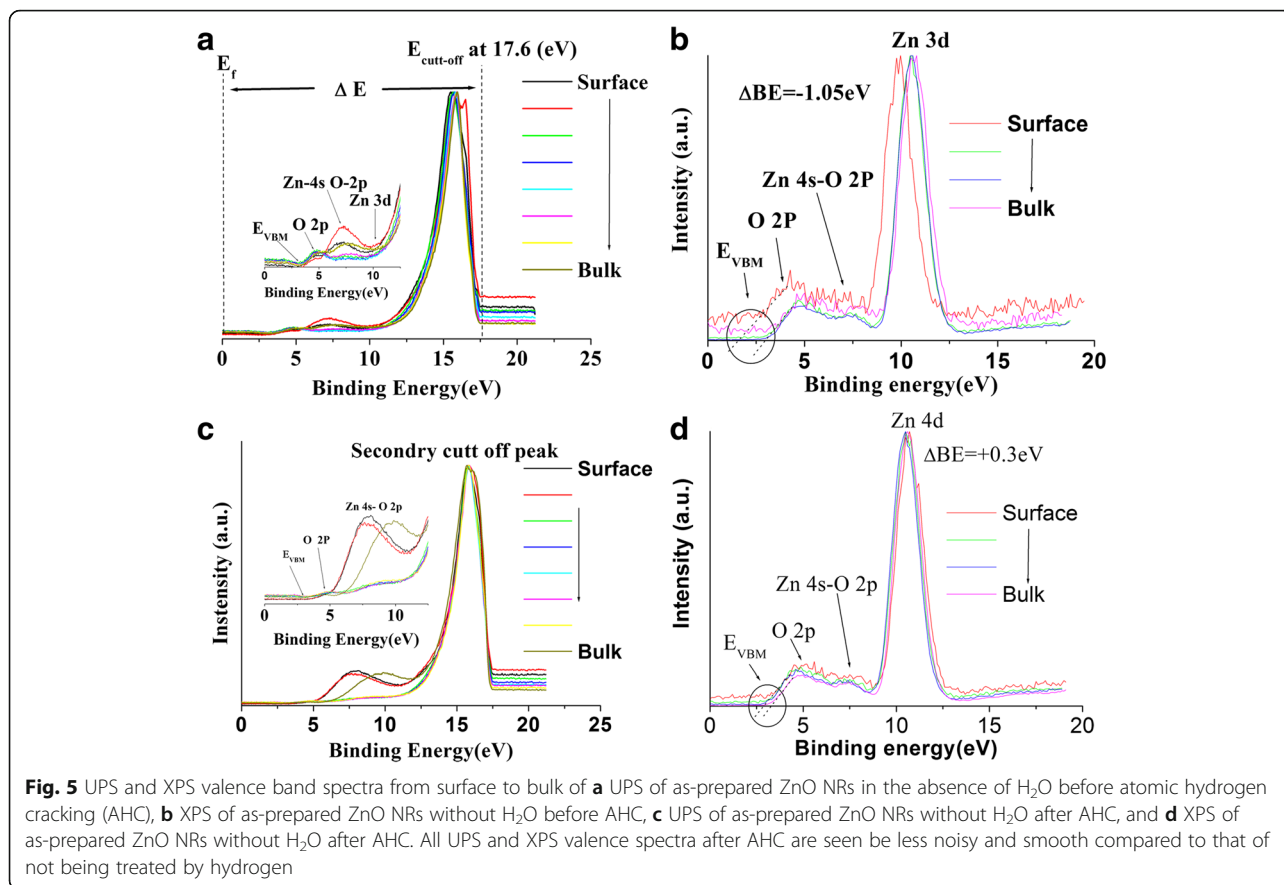Al-Saadi *et al. Nanoscale Research Letters* (2017) 12:22

Page 6 of 11

Fig. 4 O 1s XPS spectra of ZnO nanorod samples treated with hydrogen in the absence of adsorbed H_2O **a** surface, **b** sub-surface, and **c** bulk and with H_2O **d** surface, **e** sub-surface, and **f** bulk

4s-O 2p (~6–8 eV), and Zn 3d (~10.5–11.5 eV)) are detected as revealed in Fig. 5a. The inset of Fig. 5a shows slight variation from 3.3 to 2.8 eV for the E_{VBM} and attenuation of the Zn 3d peak. Taking the E_{VBM} value of 2.8 and 3.37 eV energy gap (E_g) for ZnO [22], the surface band bending (V_{sbb}) was calculated from

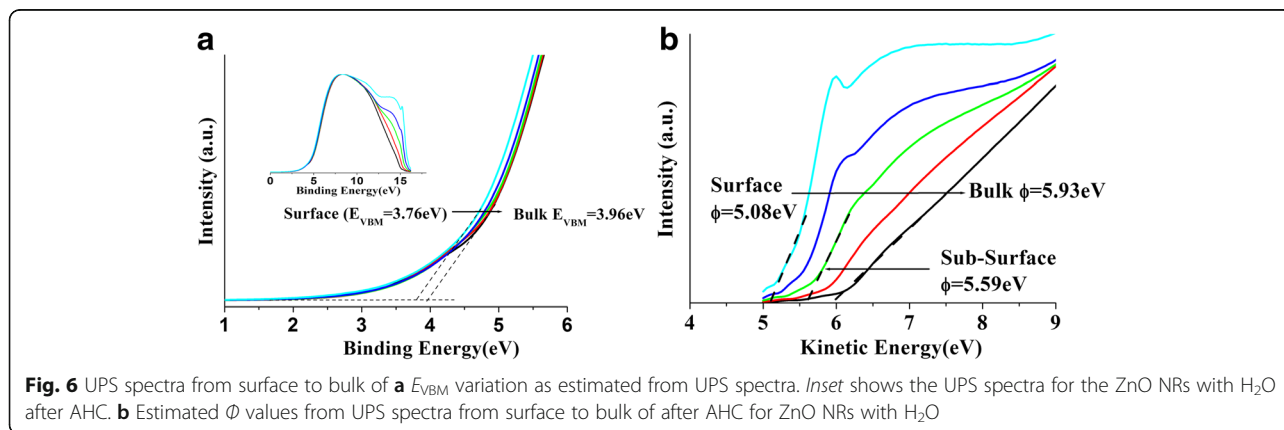$$V\text{sbb} = E_g - E_{VBM} - \Sigma \quad (1)$$

where $\Sigma = (kT/q)\ln(N_C/n)$ [34] is the energy difference between E_F and the conduction band minimum (E_{CBM}) in the bulk of the sample (n is the bulk carrier concentration 2×10^{17} cm^{-3} and N_C is the conduction band effective density of states = 2.94×10^{18} cm^{-3} for ZnO). Using these values, the Σ was found to be 0.064 eV and $V_{sbb} = 0.51$ eV. This positive V_{sbb} value is a sign of upward band bending which generates an electron depletion layer on the ZnO NRs surface and is comparable to the 0.53 eV value found by Kumarappan [20] upon H* cleaning of ZnO (0001) single crystal at high annealing temperatures. The UPS band structure features and the

decrease in E_{VBM} values are supported by the XPS valence band spectra presented in Fig. 5b. Due to the glazing angle used for XPS investigation, it is observed that the Zn 3d XPS core level—not to be confused with the secondary cutoff peak of UPS shown in Fig. 5a and E_{VBM} shift to lower binding energy value of 1.6 eV as evident in Fig. 5b. This value is attributed to surface contaminants covering the un-treated surface. As depicted in the inset of Fig. 5c and upon hydrogen treatment, the UPS O 2p peak gets attenuated and the Zn 4s-O 2p appears with enhanced intensity as the main feature related to the hydrogen treatment of the ZnO sample without H_2O. The trend of band structure features after hydrogen treatment is clearly supported by XPS valence band data shown in Fig. 5d. For example, E_{VBM} values estimated from Fig. 5d show a decrease from 3.3 to 2.8 eV moving from bulk to surface geometry. The large E_{VBM} value of 3.3 eV confirms an upward band bending and is close to the band gap (3.37 eV) of ZnO. Furthermore, this value is expected from the maximum XPS sampling depth (d) of ~10 nm estimated

Al-Saadi *et al. Nanoscale Research Letters* (2017) 12:22

Page 7 of 11

Fig. 5 UPS and XPS valence band spectra from surface to bulk of **a** UPS of as-prepared ZnO NRs in the absence of H_2O before atomic hydrogen cracking (AHC), **b** XPS of as-prepared ZnO NRs without H_2O before AHC, **c** UPS of as-prepared ZnO NRs without H_2O after AHC, and **d** XPS of as-prepared ZnO NRs without H_2O after AHC. All UPS and XPS valence spectra after AHC are seen be less noisy and smooth compared to that of not being treated by hydrogen

from $3\lambda_{max} = d$, where λ_{max} is the maximum electron mean free path value equaling to 3.5 nm for the XPS Al Kα radiation used in this study. The decrease of O_b, attenuation of the UPS O 2p peak, intensity enhancement of Zn 4s-O 2p, and enhanced smoothness of all UPS and XPS spectra after hydrogen treatment strongly strengthen the conclusion that hydrogen treatment does have a cleaning effect on the ZnO NR sample in the absence of H_2O.

Electronic band structure results obtained from the analysis of the UPS data after hydrogen treatment from the sample with H_2O show different behavior from that without H_2O. The sample with H_2O shows that there are some energy states like Zn 4s-O 2p and Zn 3d (see black spectrum in Fig. 2f) which totally disappears after treatment with hydrogen for 2 h as shown in the inset of Fig. 6a. This could be because of the layer formed on the surface of the rods by hydrogen interacting with O_b

Fig. 6 UPS spectra from surface to bulk of **a** E_{VBM} variation as estimated from UPS spectra. *Inset* shows the UPS spectra for the ZnO NRs with H_2O after AHC. **b** Estimated Φ values from UPS spectra from surface to bulk of after AHC for ZnO NRs with H_2O

mediated by the presence of O_c (i.e., adsorbed H_2O). This interaction is manifested by an increase of 13% in O_b after hydrogen treatment as seen from the comparison of O_b content in Figs. 2e and 6a. E_{VBM} decreases from 3.96 to 3.76 eV from bulk to surface as shown in the inset of Fig. 6a. Employing Eq. (1) and using the E_{VBM} value of 3.76 eV and Eg = 3.37 eV, the V_{sbb} native value of 0.45 is observed—a sign of downward band bending and the development of electron accumulation layer at the sample surface.

The work-function (Φ) can be calculated from the difference in the photon energy of He (*I*) (21.2 eV) and the energy difference ΔE between the secondary cutoff energy (E_{cutoff}) and the Fermi edge (E_F) as shown in Fig. 5a as

$$\Phi = 21.2 - \Delta E \tag{2}$$

The Φ values calculated using ΔE obtained from Fig. 5a, c are 3.6 ± 0.1 and 3.7 ± 0.1 eV before and after hydrogen exposure for the sample without adsorbed H_2O.
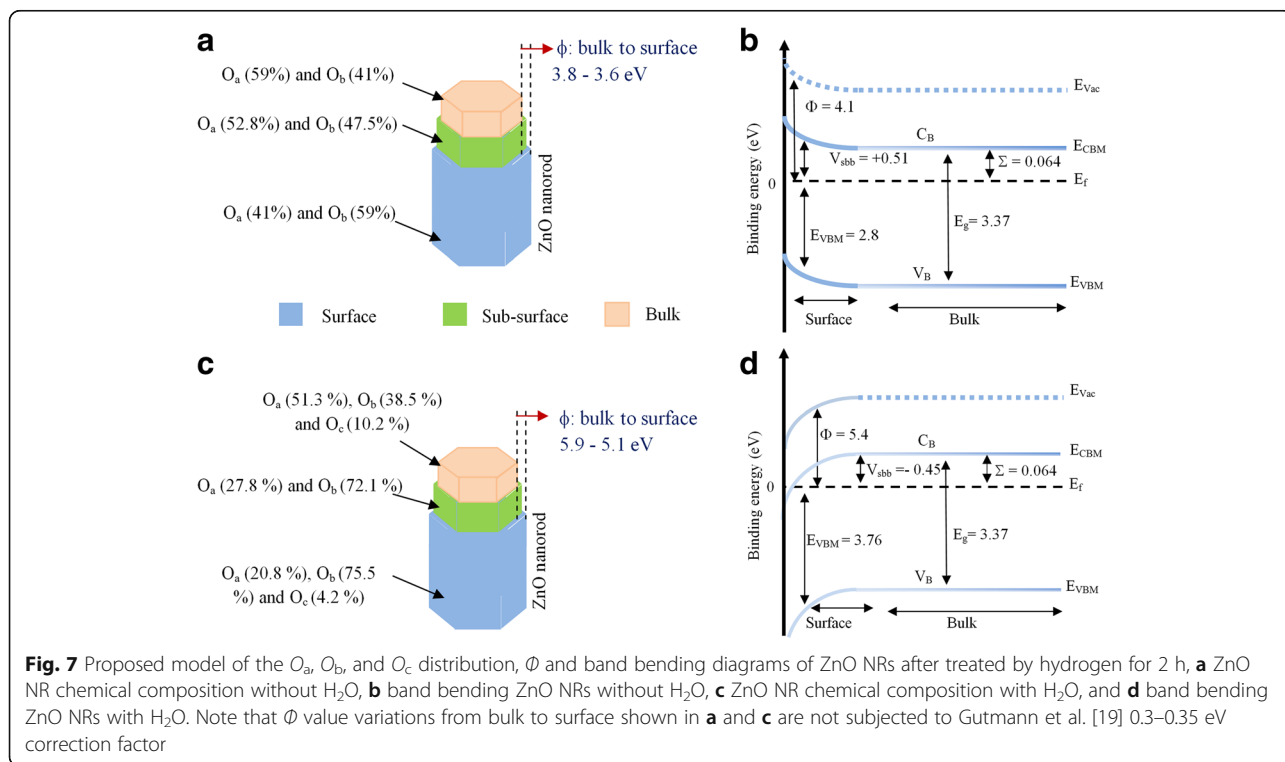
To illustrate the effect of H* treatment on the work function (Φ) for the sample with adsorbed H_2O, the UPS spectra in Fig. 6b are plotted with respect to the kinetic energy. Therefore, the extrapolated lines fitted on the secondary cutoff peaks to the energy scale directly correspond to the Φ values. Clearly, large Φ values (compared to that found in the sample without water) decreasing from 5.9 ± 0.1 to 5.1 ± 0.1 eV are found from
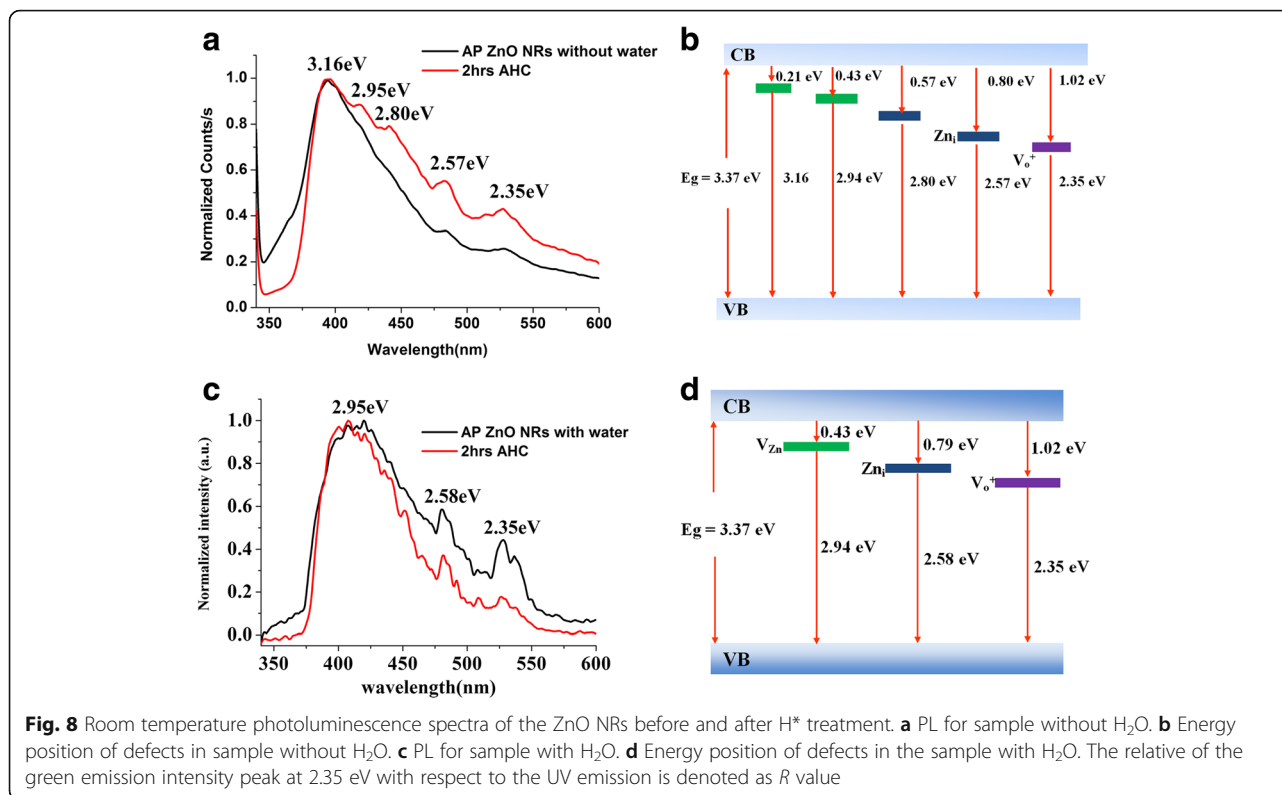
the bulk to the surface, respectively. Considering the aforementioned correction factor (0.3–0.35 eV) following the work function of Gutmann et al. [19] attributed to the effect of UV exposure during the UPS experiments, the corrected surface Φ values after H* treatment turn to be 4.0 ± 0.1 and 5.4 ± 0.1 eV for the sample without H_2O and with H_2O, respectively.

Figure 7 shows the proposed model of the surface, sub-surface and bulk chemical composition, Φ values, and band bending diagrams for the ZnO NR samples with and without H_2O content after hydrogen treatment.

It is interesting to compare the measured E_{VBM} and Φ values with those reported before. The E_{VBM} (2.8–3.3 eV) and Φ (4.1 eV) values found for the sample without water after H* treatment agree very well with published values by Kim et al. [35] (Φ = 4.08 eV) after Ar+ ion sputtering/ heating ZnO single crystal at 700 °C, Gutmann et al. [19] (E_{VBM} = 3.0 eV, Φ = 4.1 eV) on nanocrystalline ZnO surfaces after annealing at 400 °C in UHV environment, and Heinhold et al. [21] (E_{VBM} = 3.41 eV) after annealing ZnO single crystal at 750 °C for 15 min. This agreement is not surprising since annealing or Ar+ ion sputtering has similar effect of partial cleaning of ZnO as H* treatment.

Room temperature photoluminescence (PL) was recorded with the excitation wavelength of 325 nm for all samples before and after H* treatment. Figure 8a presents the data measured for the ZnO sample without H_2O before and after H* treatment. It is evident that

Fig. 7 Proposed model of the O_a, O_b, and O_c distribution, Φ and band bending diagrams of ZnO NRs after treated by hydrogen for 2 h, **a** ZnO NR chemical composition without H_2O, **b** band bending ZnO NRs without H_2O, **c** ZnO NR chemical composition with H_2O, and **d** band bending ZnO NRs with H_2O. Note that Φ value variations from bulk to surface shown in **a** and **c** are not subjected to Gutmann et al. [19] 0.3–0.35 eV correction factor

Al-Saadi *et al. Nanoscale Research Letters* (2017) 12:22

Page 9 of 11

Fig. 8 Room temperature photoluminescence spectra of the ZnO NRs before and after H* treatment. **a** PL for sample without H_2O. **b** Energy position of defects in sample without H_2O. **c** PL for sample with H_2O. **d** Energy position of defects in the sample with H_2O. The relative of the green emission intensity peak at 2.35 eV with respect to the UV emission is denoted as *R* value

after hydrogen treatment, the intensity of all emission attenuated peaks is increased due to the removal of surface contaminates with the cleaning of ZnO NR surface. The strong emission peak around 421 nm (2.94 eV) can be assigned to the recombination of an electron at zinc interstitial (Zn_i) and a hole in the valence band [36]. Two other peaks observed at 480 nm (2.58 eV) and 527 nm (2.35 eV) can be assigned as different defect state emissions [36]. Vanheusden et al. [37] had reported that the visible luminescence of ZnO mainly originate from different states such as oxygen vacancies Vo^0, Vo^+, and Vo^{+2} and Zn_i. The oxygen vacancies are located below the bottom of the conduction band (CB) in the sequence of Vo^0, Vo^+, and Vo^{+2}, from top to bottom. The peak around 527 nm can be related to singly ionized oxygen vacancy. While the green emission is a result of the recombination of the photogenerated hole with a singly ionized charged state of the specific defect. According to Anderson et al. [17] and Vanheusden et al. [37], emissions related to defects in our sample can be assigned to zinc interstitial at 480 nm (2.58 eV) as a shallow donor and singly ionized oxygen vacancy and at 527 nm (2.35 eV) as a deep donor. Zinc interstitial (Zn_i) produces a shallow donor level at 0.79 eV below the bottom of CB, and the singly ionized oxygen vacancy produces a deep donor at 1.02 eV below the bottom of CB (see Fig. 8) [38–40]. A new strong UV emission peak is found around 390 nm (3.16 eV)

attributed to ZnO–OH—supported by XPS data at binding energy of 531.2 eV in Fig. 4b—species on sub-surface of the ZnO sample without H_2O. Upon hydrogen treatment of the H_2O adsorbed on sample, the intensity of emission peaks in the visible range from 400 to 600 nm is reduced compared to what is observed for the un-treated sample. This reduction can be understood through a reaction of $H + O^{2-} \rightarrow OH^- + e^-$. The excess electrons from this reaction neutralize the positively charged oxygen vacancies thus reducing the visible PL intensity. Interestingly, the new UV peak observed at 390 nm (3.16 eV) in the sample without H_2O after H* treatment is absent in the sample with adsorbed H_2O molecules. The positions of different defect levels are schematically shown in Fig. 8b, d for the samples without H_2O and with H_2O, respectively.

It is very imperative to understand the relationship between band structure and the measured core level binding energies parameters and with the observed PL features. Table 1 shows a summary of PL *R* parameter and E_{VBM}, V_{sbb}, and Zn core-level binding energy (BE) values obtained from UPS and XPS spectra, respectively. The *R* value is defined as the relative of the green emission—it can be any emission in PL spectra—intensity peak at 2.35 eV with respect to the UV emission.

The surface band bending phenomenon seen from V_{sbb} is correlated to the estimated PL *R* values. The upward band bending reflects small *R* value (2.3) (i.e.,

Al-Saadi *et al. Nanoscale Research Letters* (2017) 12:22

Page 10 of 11

Table 1 PL *R* factor, E_{VBM} and V_{sbb} UPS parameters, and XPS Zn binding energies

Sample type	No H* treatment	With H* treatment
Sample without H_2O	$R = 4.1$, $E_{VBM} = 3.0$ eV	$R = 2.3$, $E_{VBM} = 2.8$ eV, $V_{sbb} = 0.51$ (upward)
	Zn (BE) = 1020.5 eV	Zn (BE) = 1020.8 eV
Sample with H_2O	$R = 2.2$, $E_{VBM} = 3.5$ eV	$R = 5.7$, $E_{VBM} = 3.76$ eV, $V_{sbb} = 0.45$ (downward)
	Zn (BE) = 1021.1 eV	Zn (BE) = 1021.5 eV

enhancement of PL intensity) for the sample without H_2O. However, the downward band bending induced the negative accumulation layer in the sample with H_2O, causing attenuation of PL (i.e., large *R* value 5.7).

Based on PL results, the ZnO sample without H_2O showed enhancement of defects after H* treatment. Therefore, this sample was used to study the photocatalytic degradation of phenol under solar light irradiation. The concentration of phenol at various time intervals as shown in Fig. 9 was calculated from the area under the phenol peak. In addition, the rate constant (*k*) was estimated from Fig. 9: Inset using first order pseudo kinetic model $\{-\ln(C_t/C_0) = kt\}$ where C_t is concentration of phenol at time *t* and C_0 is an initial phenol concentration. It was observed that the degradation of phenol took place in two stages: The first stage from 0–40 min and the second stage from 40–200 min with *k* values of 0.0035 ± 0.0002 and 0.00050 ± 0.00005 for ZnO and 0.00430 ± 0.00008 and 0.00080 ± 0.00005 for H*-treated ZnO, respectively. After 180 min, 24% of phenol degradation was observed for the H*-treated ZnO compared to 18% degradation in the presence of pristine ZnO nanorod sample. As a result, H* treatment of ZnO at room temperature demonstrated 25% improvement in photocatalytic degradation of phenol attributed to the surface defects. It is anticipated that the photocatalytic degradation of phenol will be further enhanced for ZnO samples treated with H* at high annealing temperatures [41].

Conclusions

Zinc oxide nanorods were synthesized on glass substrates using a hydrothermal process, and the surface defects were modulated by H* treatment at room temperature. XPS and UPS revealed the surface, sub-surface, and bulk chemical composition and electronic band structures of the ZnO samples with and without H_2O in their structure. The H* treatment had the effect of cleaning the ZnO NRs, enhancement of PL signals, upward band bending, and improved phenol degradation for the sample without H_2O. Downward band bending and attenuation of PL signal were the main features for the sample with H_2O. The reported results show that the surface, sub-surface, and bulk chemical oxygen vacancies can be correlated to the observed defects and the H_2O/H* species can be used to tailor the band bending of the ZnO NRs which might be required for several applications.

Authors' Contributions
MJA-S conducted the experiment and prepared the manuscript. SA-H, JD, and AA-H designed the experiment and reviewed the manuscript. HHK, MTZM, TB, and KL prepared and reviewed the manuscript. All authors read and approved the final manuscript.

Competing Interests
The authors declare that they have no competing interests.
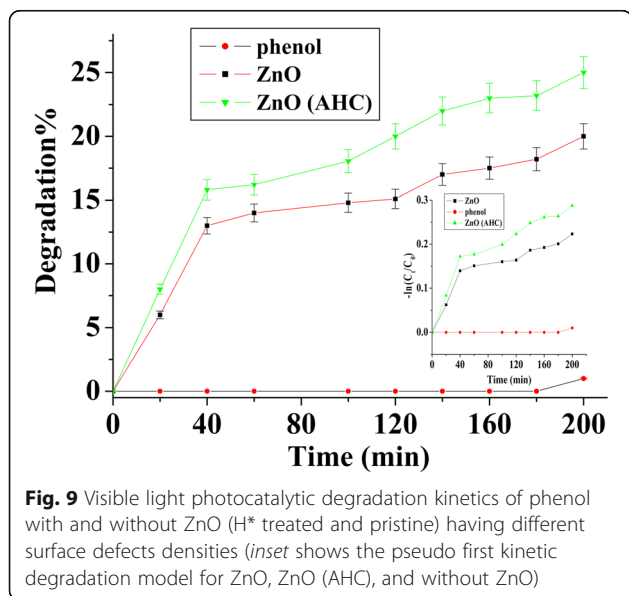
Author details
^{1}Department of Physics, Sultan Qaboos University, PO Box 36, Al Khoudh, 123, Muscat, Oman. ^{2}Chair in Nanotechnology, Water Research Center, Sultan Qaboos University, PO Box 17, Al Khoudh, 123, Muscat, Oman. ^{3}Department of Chemistry, Sultan Qaboos University, PO Box 36, Al Khoudh, 123, Muscat, Oman. ^{4}Functional Materials Division, Materials and Nanophysics, ICT School, KTH Royal Institute of Technology, Isafjordsgatan 22, SE-164 40 Kista, Stockholm, Sweden.

References
1. Blumenstein NJ, Berson J, Walheim S, Atanasova P, Baier J, Bill J et al (2015) Template-controlled mineralization: determining film granularity and structure by surface functionality patterns. Beilstein J Nanotechnol 6:1763–8
2. Xia JB, Zhang XW (2006) Electronic structure of ZnO wurtzite quantum wires. Eur Phys J B 49(4):415–20

Fig. 9 Visible light photocatalytic degradation kinetics of phenol with and without ZnO (H* treated and pristine) having different surface defects densities (*inset* shows the pseudo first kinetic degradation model for ZnO, ZnO (AHC), and without ZnO)

Al-Saadi et al. Nanoscale Research Letters (2017) 12:22

Page 11 of 11

3. Sunandan B, Joydeep D (2009) Hydrothermal growth of ZnO nanostructures. Sci Technol Adv Mater 10(1):013001

4. Ye J, Gu S, Qin F, Zhu S, Liu S, Zhou X et al (2005) Correlation between green luminescence and morphology evolution of ZnO films. Appl Phys A 81(4):759–62

5. Alvi NH, Ul Hasan K, Nur O, Willander M (2011) The origin of the red emission in n-ZnO nanotubes/p-GaN white light emitting diodes. Nanoscale Res Lett 6(1):130

6. Baruah S, Mahmood MA, Myint MTZ, Bora T, Dutta J (2010) Enhanced visible light photocatalysis through fast crystallization of zinc oxide nanorods. Beilstein J Nanotechnol 1:14–20

7. Bora T, Lakshman KK, Sarkar S, Makhal A, Sardar S, Pal SK et al (2013) Modulation of defect-mediated energy transfer from ZnO nanoparticles for the photocatalytic degradation of bilirubin. Beilstein J Nanotechnol 4(1):714–25

8. Khayatian A, Kashi MA, Azimirad R, Safa S, Akhtarian SFA (2016) Effect of annealing process in tuning of defects in ZnO nanorods and their application in UV photodetectors. Optik - Int J Light Electron Opt 127(11):4675–81

9. Akhavan O, Mehrabian M, Mirabbaszadeh K, Azimirad R. (2009) Hydrothermal synthesis of ZnO nanorod arrays for photocatalytic inactivation of bacteria. J Phys D Appl Phys. 42(22): 225305-14

10. Wei S, Lian J, Wu H (2010) Annealing effect on the photoluminescence properties of ZnO nanorod array prepared by a PLD-assistant wet chemical method. Mater Charact 61(11):1239–44

11. Viter R, Iatsunskyi I, Fedorenko V, Tumenas S, Balevicius Z, Ramanavicius A et al (2016) Enhancement of electronic and optical properties of ZnO/Al2O3 nanolaminate coated electrospun nanofibers. J Phys Chem C 120(9):5124–32

12. Maffeis TGG, Penny MW, Castaing A, Guy OJ, Wilks SP (2012) XPS investigation of vacuum annealed vertically aligned ultralong ZnO nanowires. Surf Sci 606(1–2):99

13. Tam KH, Cheung CK, Leung YH, Djurišić AB, Ling CC, Beling CD et al (2006) Defects in ZnO nanorods prepared by a hydrothermal method. J Phys Chem B 110(42):20865–71

14. Chin-Ming Hsu C-HC, Wen-Tuan W (2009) Molybdenum doped zinc oxide films with enhanced electrical conductivity by hydrogen plasma treatment. In: International Conference on Optics and Photonics in Taiwan

15. Hooyoung Song J-HK, Kim EK, Ha J, Hong JP (2008) Hydrogen plasma treatment Of ZnO thin films grown by using laser deposition. J Korean Phys Soc 53:2540–3

16. Lin CC, Chen HP, Liao HC, Chen SY (2005) Enhanced luminescent and electrical properties of hydrogen-plasma ZnO nanorods grown on wafer-scale flexible substrates. Appl Phys Lett 86(18):1–3

17. Janotti A, Van de Walle CG (2006) New insights into the role of native point defects in ZnO. J Cryst Growth 287(1):58–65

18. Yin J, Gao F, Wei C, Lu Q (2014) Water amount dependence on morphologies and properties of ZnO nanostructures in double-solvent system. Sci Rep 4:3736

19. Gutmann S, Conrad M, Wolak MA, Beerbom MM, Schlaf R (2012) Work function measurements on nano-crystalline zinc oxide surfaces. J Appl Phys 111(12):123710

20. Kumarappan K. PhD thesis. Dublin City University 2014.

21. Heinhold R, Williams GT, Cooil SP, Evans DA, Allen MW (2013) Influence of polarity and hydroxyl termination on the band bending at ZnO surfaces. Phys Rev B 88(23):235315

22. Mahmood MA, Dutta J (2011) Spray pyrolized pre-coating layers for controlled growth of zinc oxide nanorods by hydrothermal process. Nanotechnol Nanosci 1(2):92–6

23. Mahmood MA, Bora T, Dutta J (2013) Studies on hydrothermally synthesised zinc oxide nanorod arrays for their enhanced visible light photocatalysis. Int J Environ Technol Manag 16(1–2):146–59

24. Sugunan A, Warad HC, Boman M, Dutta J (2006) Zinc oxide nanowires in chemical bath on seeded substrates: role of hexamine. J Sol-Gel Sci Technol 39(1):49–56

25. Baruah S, Dutta J (2009) Effect of seeded substrates on hydrothermally grown ZnO nanorods. J Sol-Gel Sci Technol 50(3):456–64

26. Baruah S, Dutta J (2009) pH-dependent growth of zinc oxide nanorods. J Cryst Growth 311(8):2549–54

27. Myint MTZ, Kumar NS, Hornyak GL, Dutta J (2012) Hydrophobic/hydrophilic switching on zinc oxide micro-textured surface. Appl Surf Sci 264:344–8

28. Park Y, Choong V, Gao Y, Hsieh BR, Tang CW (1996) Work function of indium tin oxide transparent conductor measured by photoelectron spectroscopy. Appl Phys Lett 68(19):2699–701

29. Myint MTZ, Dutta J (2012) Fabrication of zinc oxide nanorods modified activated carbon cloth electrode for desalination of brackish water using capacitive deionization approach. Desalination 305:24–30

30. Byrne D, McGlynn E, Henry MO, Kumar K, Hughes G (2010) A novel, substrate independent three-step process for the growth of uniform ZnO nanorod arrays. Thin Solid Films 518(16):4489–92

31. Shet S, Ahn K-S, Deutsch T, Wang H, Nuggehalli R, Yan Y et al (2010) Influence of gas ambient on the synthesis of co-doped ZnO:(Al, N) films for photoelectrochemical water splitting. J Power Sources 195(17):5801–5

32. Ye Z-Z, Zhu-Ge F, Lu J-G, Zhang Z-H, Zhu L-P, Zhao B-H et al (2004) Preparation of p-type ZnO films by Al+N-codoping method. J Cryst Growth 265(1–2):127

33. Liu T, He X, Zhang J, Feng L, Wu L, Li W et al (2012) Effect of ZnO films on CdTe solar cells. J Semicond 33(9):093003

34. Heinhold R, Reeves RJ, Williams GT, Evans DA, Allen MW (2015) Mobility of indium on the ZnO(0001) surface. Appl Phys Lett 106(5):051606

35. Kim T, Yoshitake M, Yagyu S, Nemsak S, Nagata T, Chikyow T (2010) XPS study on band alignment at Pt-O-terminated ZnO (0001) interface. Surf Interface Anal 42(10–11):1528–31

36. Samanta SKP PK, Ghosh A, Roy Chanudhrui P (2009) Visible emission from ZnO nanorods synthesized by a simple wet chemical method. Int J Nanotechnol Nanosci 1:81–90

37. Vanheusden K, Seager CH, Warren WL, Tallant DR, Voigt JA (1996) Correlation between photoluminescence and oxygen vacancies in ZnO phosphors. Appl Phys Lett 68(3):403–5

38. Xu PS, Sun YM, Shi CS, Xu FQ, Pan HB (2003) The electronic structure and spectral properties of ZnO and its defects. Nucl Inst Methods Phys Res B 199:286–90

39. Zhang SB, Wei SH, Zunger A (2001) Intrinsic n-type versus p-type doping asymmetry and the defect physics of ZnO. Phys Rev B 63(7):075205

40. Chen Y, Bagnall DM, Zhu Z, Sekiuchi T, Park K-t, Hiraga K et al (1997) Growth of ZnO single crystal thin films on c-plane (0 0 0 1) sapphire by plasma enhanced molecular beam epitaxy. J Cryst Growth 181(1–2):165–9

41. Al-Sabahi J, Bora T, Al-Abri M, Dutta J (2016) Controlled defects of zinc oxide nanorods for efficient visible light photocatalytic degradation of phenol. Materials 9(4):238